JMEPEG (2022) 31:5812–5822
https://doi.org/10.1007/s11665-022-06626-6

1059-9495/$19.00

TECHNICAL ARTICLE

Surface Friction and Wear Behavior of In Situ AlB_2 Particle-Reinforced A356 Composites

Lei Jiao, Fan Li, Yutao Zhao, BaoWang Wang, XinPeng Huang, Hui Li, Tao Wu, and Likun Cao

Submitted: 21 June 2021 / Revised: 26 November 2021 / Accepted: 30 November 2021 / Published online: 14 February 2022

A new A356-KBF4 system was established and AlB_2 particles reinforced A356 composite was prepared by melt direct reaction method. The effect of AlB2 particle content on the structure and tribological properties of the material was studied by scanning electron microscope, microhardness and tribological wear tests. The hardness of AlB_2/A356 composite is up to 213.4728Hv. The friction coefficient and wear rate of A356 alloy decreased with the addition of AlB_2.

Keywords aluminum matrix composites, AlB_2 particles, in situ synthesis, tribological behavior

1. Introduction

As a commonly used high-strength aluminum alloy that can be heat-treated and strengthened, A356 aluminum alloy has the advantages of excellent casting performance, high specific strength, high wear resistance and low cost. Because of its excellent casting properties, it is widely used in some parts that require the high wear resistance of alloys. (Ref 1-3).

After decades of verification, the liquid casting method is the most economical method for preparing aluminum matrix composites. However, the aluminum-based composite material prepared by the liquid casting method has the disadvantage of uneven particle agglomeration distribution. In order to avoid this situation, the magnetic field stirring method, ultrasonic vibration method and semisolid stirring method can be used in the liquid casting process (Ref 4-6).

At present, the use of reinforced particles to prepare aluminum matrix composites is a standard method to enhance the properties of aluminum alloys (Ref 7-12). The in situ endogenous particles have attracted more and more attention due to the high degree of clean combination with the substrate (Ref 13-18). The most commonly used particle reinforcement materials in pure aluminum or alloys include SiC, ZrB_2, TiB_2, Al_2O_3 and Al_3Zr (Ref 19-22). In previous studies, Mozammil et al. (Ref 23) prepared Al-4.5%Cu-xTiB_2 (x = 3, 6, 9 ,and 12 wt.%) through in situ reaction and stirring casting technology for the first time, revealing the titanium/boron in aluminum-copper alloys the mechanism of phase evolution, especially the influence on its mechanical behavior. Zhang et al. (Ref 24) used the in situ magnetochemical method to prepare (Al_2O_3+Al_3Zr)/A356 nanocomposites to study the effect of particle-matrix interface bonding on the mechanical properties of the composites. Qian (Ref 25) et al. used the in situ reaction method to prepare (ZrB2+TiB2)/6082Al and added the rare earth element Er to study the effect of the synergistic effect of the reinforcing particles and the rare earth element on the microstructure and mechanical properties of the composite material.

Similarly, many reinforcing phases can further enhance the friction and wear behavior of A356 aluminum alloy (Ref 26). Benyamin ABBASIPOUR and others (Ref 27) used melt stirring, rheological casting, stirring casting and composite casting techniques to prepare melt stirring, rheological casting, stirring casting and composite casting technologies to improve the wear resistance of A356 alloy. Janbozorgi et al. (Ref 28) has studied the effect of molybdenum disulfide lubricating particles on the friction and wear behavior of aluminum alloys.

Among many reinforcement particles, AlB_2 reinforcement particles are used as effective nucleation sites for aluminum alloys (Ref 29-31), but there are few studies on them. The layered structure of AlB_2, similar to graphite, may have a significant impact on optimizing the friction and wear behavior of A356. In this study, an in situ AlB2 particle-reinforced A356 aluminum alloy composite was prepared by developing a new A356-KBF4 system. And analyzed its microstructure to study its tribological behavior

2. Experimental Process

2.1 Preparation for Composites

$x$wt.% AlB_2/A356(x = 3, 6, 9, 12) composite was prepared from industrial A356 alloy ingot and KBF_4 inorganic salt powder. A356 alloy ingots and KBF_4 inorganic salt powder were dried at 523K for 2h. A356 alloy ingot was melted and heated to 1143K in a resistance furnace, and then KBF_4 inorganic salt powder was added. The graphite bell jar is used to press KBF_4 inorganic salt powder into the melt to avoid flotation. The graphite rod was used for stirring and reaction for 30min, and then the slag was removed. When the melt temperature dropped to 993K, the melt was cast into the iron

Lei Jiao, Fan Li, Yutao Zhao, BaoWang Wang, XinPeng Huang, Tao Wu, and **Likun Cao**, School of Materials Science and Engineering, Jiangsu University, Zhenjiang 212013, China; **Hui Li**, School of Materials Science and Engineering, Jiangsu University of Science and Technology, Zhenjiang 212003, China. Contact e-mails: jiaolei@ujs.edu.cn, lifan970814@163.com, zhaoyt@mail.ujs.edu.cn.

mold to obtain the AlB_2/A356 composite material. The *x*wt.% AlB_2/A356(x = 3, 6, 9, 12) composite was obtained by repeating the above experiment for four times.

2.2 Hardness Testing

The hardness test sample is a 10mm*10mm*10mm cube. Vickers hardness machine was used for hardness testing. Under the condition of pressure of 2 N, each sample was tested ten times to get the average of experimental results.

2.3 Tribological Behavior

The samples used 15mm*15mm*3mm cuboid made by SYJ-400 cutting machine. The friction and wear sample and Si_3N_4 are selected as the friction pair, and the friction and wear test of the sample is carried out by the HT-1000 friction and wear tester. The matrix A356 alloy and AlB_2/A356 (x = 3, 6, 9, 12) composites were tested for friction and wear behaviors under 5, 10 and 15 N normal load and 200 rpm rotational speed for 30 min. Additionally, the matrix alloy and all composites were tested for friction and wear under 10 N load for 30 min. at rotational speeds of 250 and 300 rpm. Test wear scars are analyzed by LEXTOLS400 confocal laser scanning microscope. The experiment was carried out three times to get the experimental results. The wear rate (the volume worn under unit load per unit length) is calculated by formula (1).

$$K = \frac{C \times S}{F \times L} \quad \text{(Eq 1)}$$

2.4 Characterization

The metallographic sample is a cube of 10mm * 10mm * 10mm processed by the SYJ-400 cutting machine. The sample was sanded and polished with 1500-mesh sandpaper. The micro morphology of the material was analyzed by scanning electron microscope (SEM, Carl Zeiss Merlin, Germany) and energy dispersive spectrometer (EDS). Phase analysis was performed by x-ray diffraction (XRD, BRUKER D8 ADVANCE XRD, Germany), and the crystal grain morphology was observed by polarizing microscope (PC, LEICA ICC50 W, Germany).

3. Results and Discussion

3.1 XRD Analysis

Figure 1 shows the XRD pattern of A356 alloy and *x*wt.%AlB2/A356 composite material.

It can be clearly seen from the figure that the XRD pattern of *x*wt.% AlB_2/A356 composite shows the diffraction peak of AlB2.In contrast, the XRD pattern of A356 does not show the diffraction peak of AlB_2, indicating that AlB_2 particles have been successfully synthesized. According to the literature, we have obtained the reaction equation of AlB_2 (Ref 32) formation as:

$$2KBF4 + 3Al = AlB2 + 3KAlF4 \quad \text{(Eq 2)}$$

The plane spacing between AlB_2 and Al is obtained by MDI Jade 6 software. According to formula (3), the mismatch between AlB_2 and Al matrix is calculated to be 3.76%,

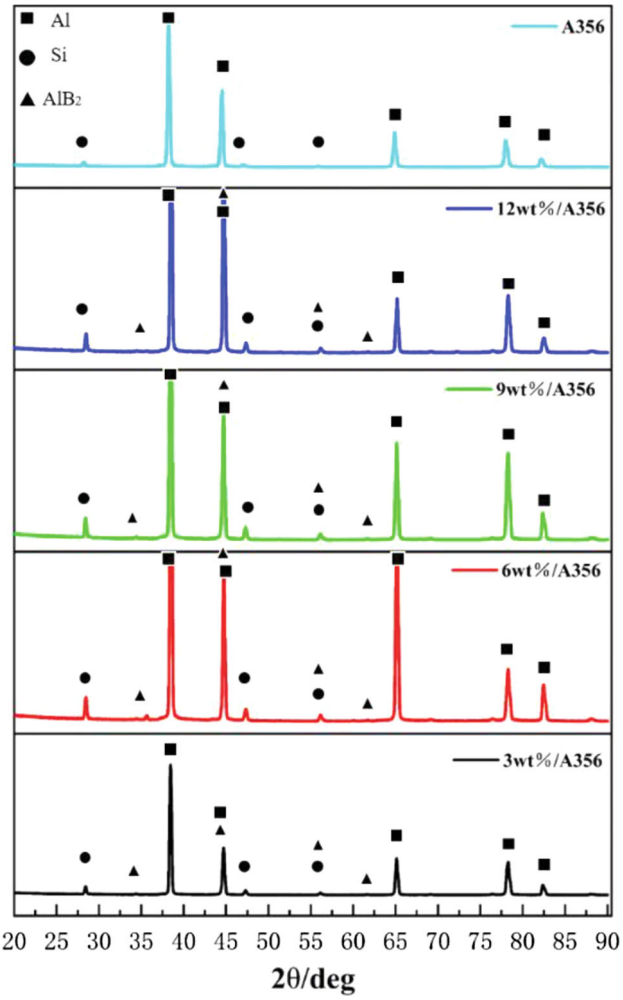

Fig. 1 XRD pattern of xwt.%AlB_2/A356 (x = 3, 6, 9, 12)

indicating that AlB_2 particles have a specific refining effect on Al grains.

$$\delta_{(hkl)_n}^{(hkl)_s} = \frac{1}{3}\sum_{i=1}^{3}\frac{\left|d(uvw)_s^i \cos\theta - d(uvw)_n^i\right|}{d(uvw)_n^i} \times 100\% \quad \text{(Eq 3)}$$

3.2 Microstructure Morphology

Figure 2 shows the scanned image and EDS energy spectrum of A356 composites with different contents of AlB_2 particles. The marked area is the EDS scanning area. The results of EDS can once again verify the successful synthesis of AlB_2 particles. From four SEM pictures, you can see different content AlB2 particles, and most of the AlB_2 particles are mainly rod-shaped, and there are some square and hexagonal particles. It can be seen from Fig. 2(d) that when x = 12, the AlB_2 particles have an obvious aggregation tendency compared to Fig. 2(a), (b), (c), which may have different effects on the performance of the composite material positive effect.

Figure 3 shows a polarization micrograph of A356 matrix and composite material. It can be clearly seen from Fig. 3 that the addition of AlB_2 has a refining effect on Al grains. This may be because AlB_2 particles can be used as effective nucleation sites for aluminum alloys and have a good refining effect on aluminum alloy grains. This is consistent with the low mismatch between

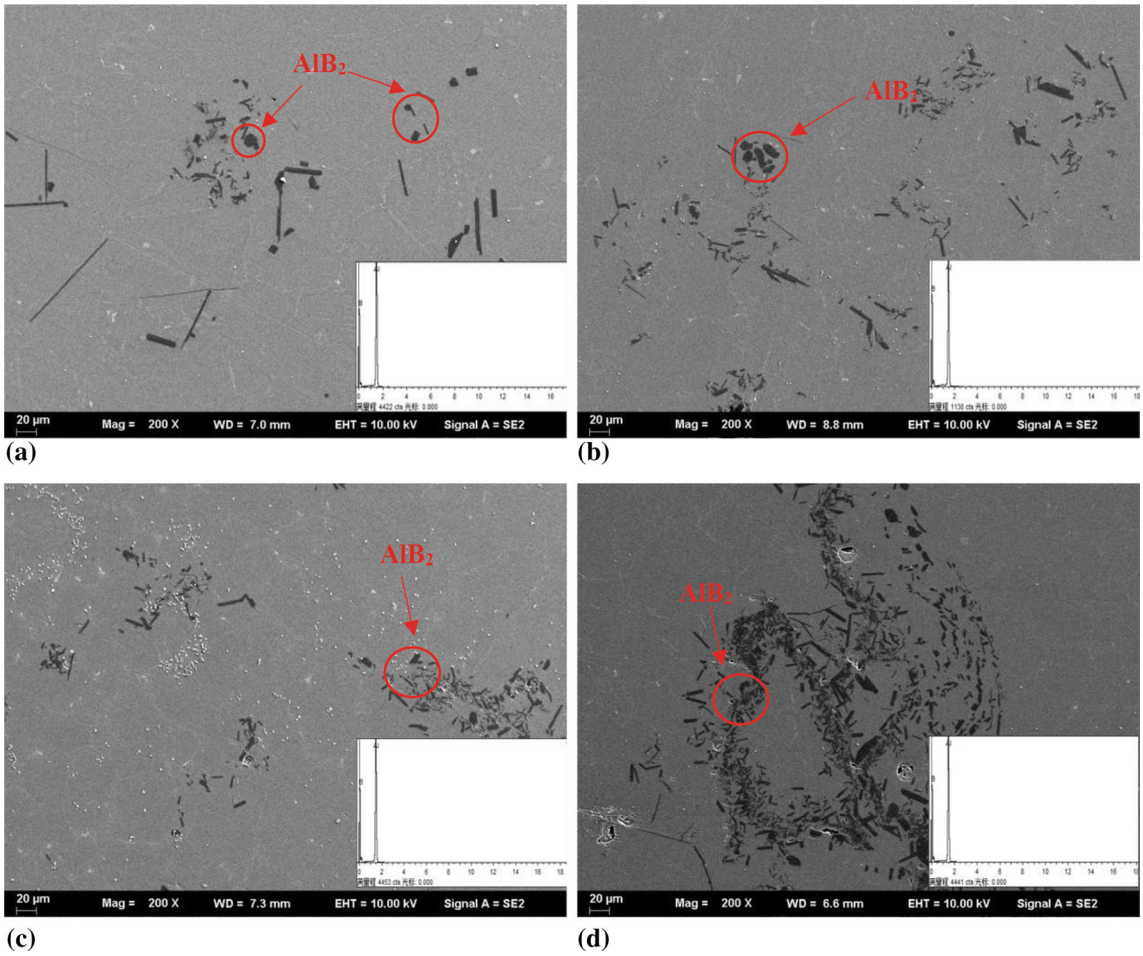

Fig. 2 SEM and EDS images of the A356 matrix composites reinforced by different content of AlB_2 particles: (a): 3wt.% (b): 6wt.% (c): 9wt.% (d): 12wt.%

AlB_2 particles and Al. The grain size was measured with image pro plus 6.0 software, and the measurement results are plotted in Fig. 4. It can be seen from Fig. 4 that when $x = 9$, the grain size reaches the minimum value of 28.5847 μm, and when $x = 12$, the refinement effect becomes worse. This may be due to the excessive agglomeration of AlB_2 particles, resulting in poor refinement effect. Figure 5 shows the Vickers hardness of different materials. The hardness change trend shown in Fig. 5 is basically the same as the material grain size change trend. When $x = 9$, the hardness of the composite material reaches the highest 213.4728Hv. This may be due to the fact that finer grains prevent the propagation of cracks and increase the hardness, which may also optimize the tribological behavior of the material.

3.3 Coefficient of Friction

3.3.1 The Effect of Load and Rotating Speed on Friction Coefficient. Figure 6 and 7 shows the variation curves of the friction coefficient of A356 alloy and xwt.% AlB_2/A356 composite with load and speed, respectively. It can be seen from Fig. 6 and 7 that the addition of AlB_2 particles has a certain anti-friction effect on the material. This may be due to the fact that AlB_2 particles act as a buffer layer in the matrix. Under different loads and different speeds, as x increases from 3 to 12, the friction coefficient of the composite material is reduced by an average of 24.7522, 19.7487, 20.4625, 18.2248% (load), 18.682, 16.7896, 17.8286, 10.6755% (rotation speed) compared with the A356 alloy matrix. This indicates that in the friction test, the dispersion of AlB2 particles on the surface of the composite material has an important effect on the friction coefficient of the material. As the content of AlB_2 particles increases, AlB_2 particles tend to agglomerate, and the agglomeration of AlB_2 particles results in a relatively rough surface of the composite material. This may be the reason for the best anti-friction effect when $x = 3$. It can be seen from Fig. 6 that as the load increases, the friction coefficient of the material shows a downward trend. It is assumed that as the load increases, the friction and wear mechanism changes from adhesive wear to abrasive wear, which reduces the friction strength and reduces the friction coefficient. It can be seen from Fig. 7 that as the speed increases, the friction coefficient curve becomes relatively unstable, and when the speed is as high as 300 rpm, the friction coefficient tends to increase. This may be because the increase in speed causes a lot of friction during the friction process. The frictional heat produces more oxides, which affects the indicated roughness. And the friction and wear mechanism becomes oxidative wear.

3.3.2 Effect of Load on Wear Rate. Figure 8 and 9 shows the wear volume and wear rate of xwt.% AlB_2/A356 composite and A356 alloy under different loads. It can be seen

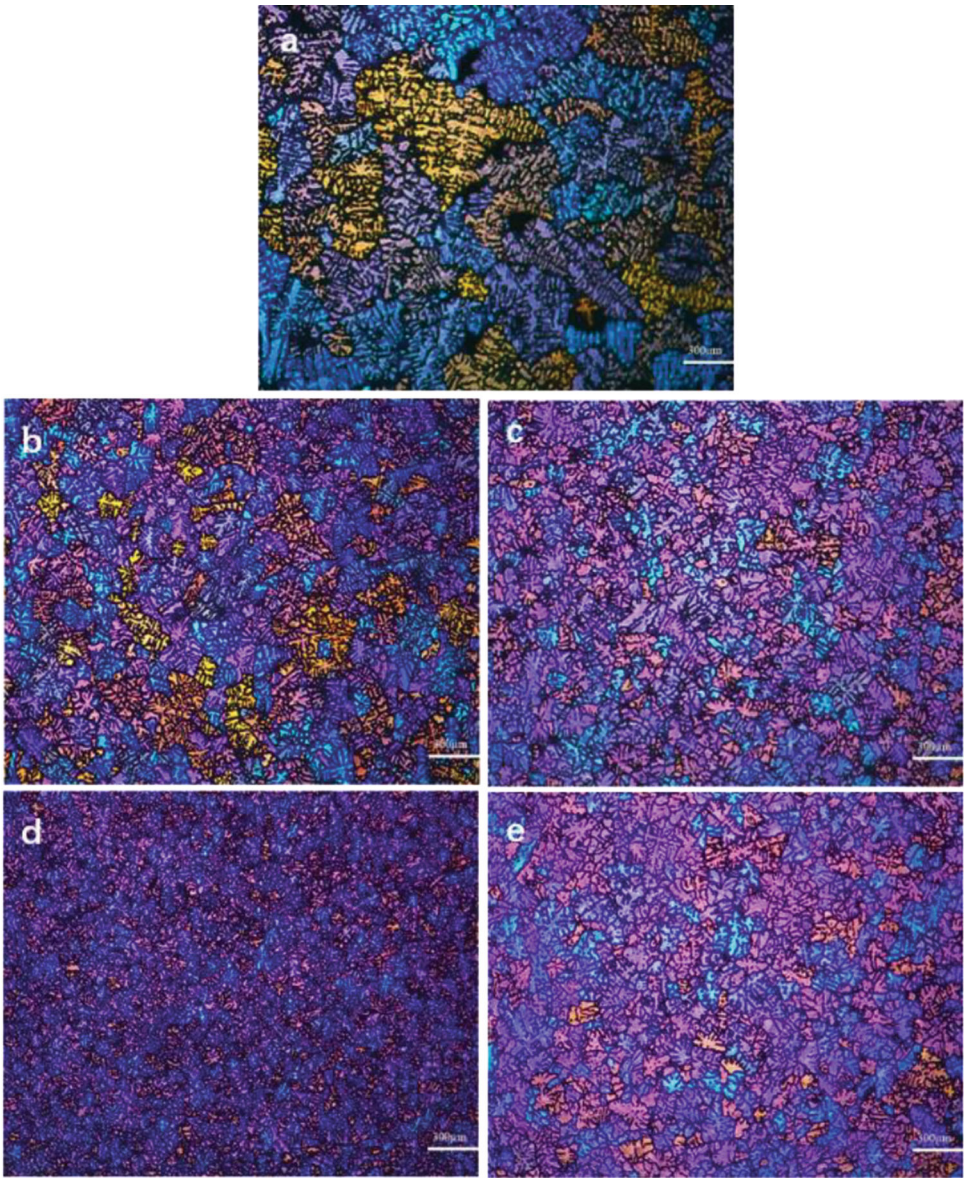

Fig. 3 PC images of the A356 matrix composites reinforced by different content of AlB_2 particles: (a): A356 (b): 3wt.% (c): 6wt.% (d): 9wt.% (e): 12wt.%

from Fig. 8 and 9 that the amount of wear of all materials increases to a certain extent with the increase of load. Under the same load, the amount of wear and wear rate of the composite material added with AlB_2 particles are lower than that of the A356 alloy. This shows that the addition of AlB_2 particles significantly improves the wear resistance of the material. Under the same load, when $x = 9$, compared with A356 alloy, the wear rate of the composite material is reduced by 22.9671% (5 N), 31.2032% (10N) and 33.4922% (15N). The wear rate reflects the amount of wear under a unit load per unit length. It can be seen from Fig. 9 that almost all materials decrease as the load increases. As can be seen from Fig. 9, wear rates of almost all materials decrease with the increase of load. This shows that the amount of wear and load in the same time is not proportional to the relationship. It may be that during the wear process, the peeling material worn by the adhesive is welded to the material surface, and the wear rate is reduced. Figure 10 shows a scanning electron microscope analysis of the wear morphology of A356 alloy and 9wt.% AlB_2/A356 composite under different loads. From Fig. 10 (a), b), (c), it can be clearly seen that there is a large peeling layer. This is because as the load increases, the cracks on the subsurface of the A356 alloy also increase, resulting in a large amount of peeling, and the main wear mechanism is adhesive wear. In Fig. 10 (e), (f), (g), the wear pattern of 9wt.% AlB_2/A356 composite is flatter than that of A356 alloy. The obvious grooves and some small exfoliated layers indicate that the wear mechanism is mainly abrasive wear and slight adhesive wear.

3.3.3 Effect of Load on Wear Rate. Figure 11 and 12 shows the wear amount and wear rate of xwt.% AlB_2/A356 composite and A356 alloy at different rotation speeds. Like the wear under different loads, the wear of all materials increases to a certain extent with the increase of the speed, and the wear of the composite material at the same speed is lower than that of

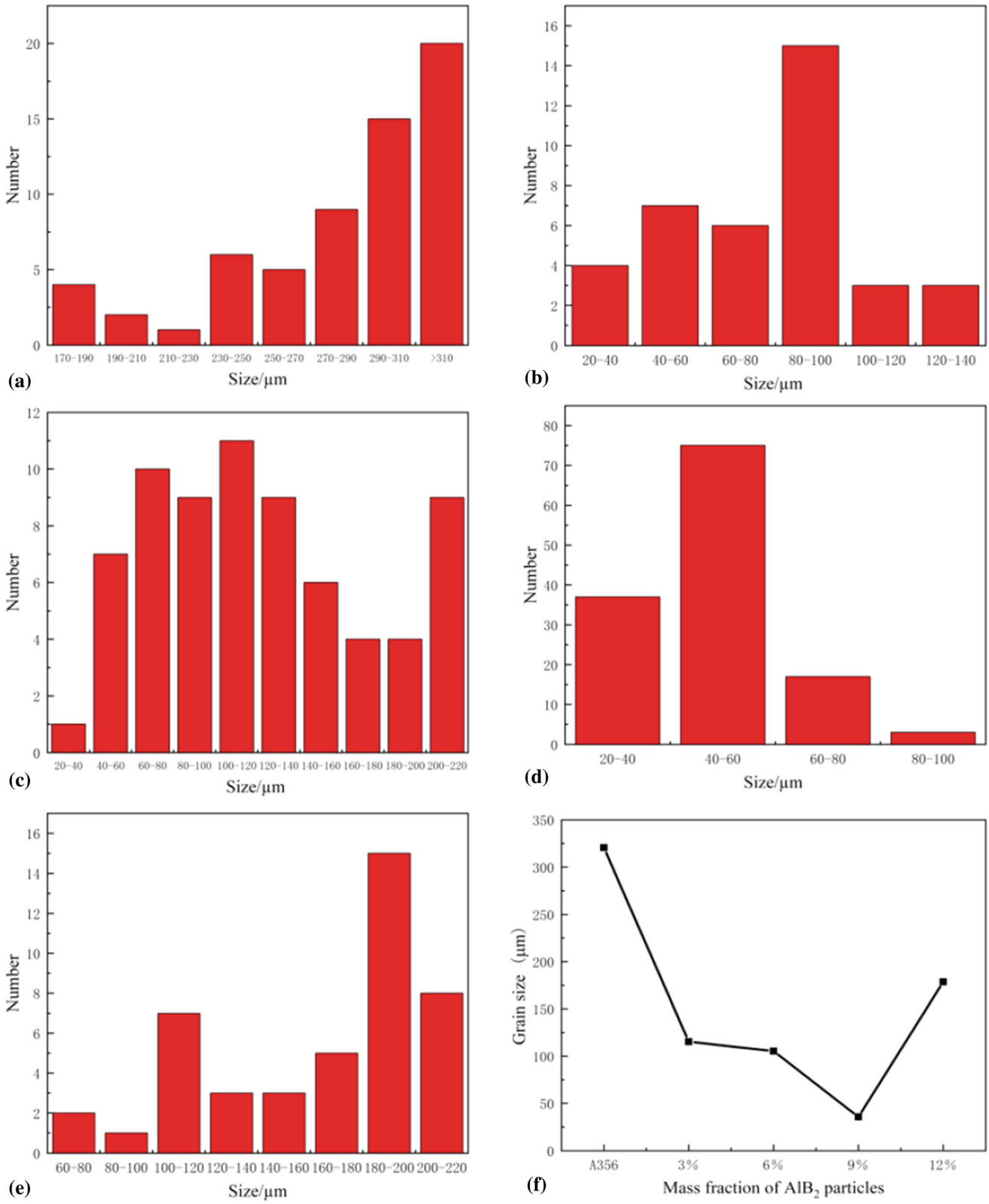

Fig. 4 Grain size of the A356 matrix composites reinforced by different content of AlB_2 particles: (a):A356 (b): 3wt.% (c): 6wt.% (d): 9wt.% (e): 12wt.% (f): average size

the A356 alloy. Under different loads or different speeds, the addition of AlB_2 particles is conducive to improving the wear resistance of the material. When $x = 9$, compared with A356 alloy, the wear of the composite material is reduced the most, reaching 31.2032% (200rpm), 27.2298% (250rpm), 28.4187% (300rpm). Unlike wear under different loads, as the speed

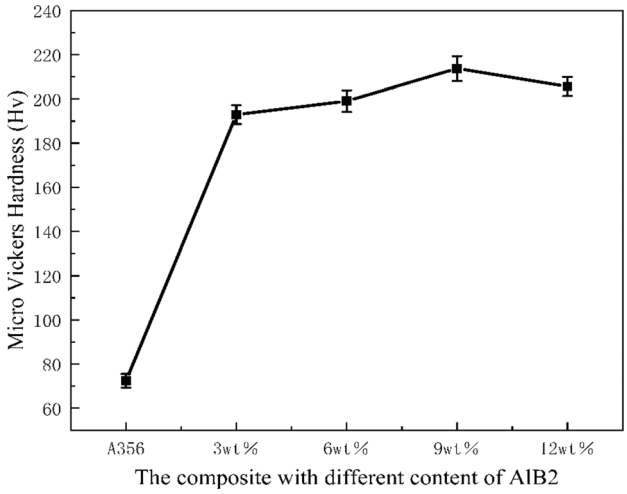

Fig. 5 The Micro Vickers Hardness of the matrix and the *x*wt.%/A356 composite

increases, the wear rate of almost all materials increases. Figure.13 shows the wear morphology of A356 alloy and 9wt.% AlB_2/A356 composite. It can be seen from Fig. 13(a), (b), (c) that the wear morphology of A356 alloy has severe subsurface fracture, and obvious oxides can be seen in the wear morphology. EDS energy spectrum analysis was performed on the wear form. It is not difficult to see that the oxygen content indicated by wear increases with the increase in speed. When the speed is increased to 300rpm, the main mechanism of A356 alloy wear is oxidative wear. This may be due to the high-speed generation of a large amount of frictional heat, which makes the A356 alloy more susceptible to oxidation. In Fig. 13(d), (e), (f), it can be seen that the wear of the 9wt.% AlB_2/A356 composite shows no subsurface fracture. Some oxides and furrows indicate that the wear mechanism is oxidative wear and abrasive wear. It can be seen from the EDS energy spectrum that the oxygen content of the worn surface is not as high as that of the A356 alloy. This may be because (1): AlB_2 refines the crystal grains of the matrix, so that the hardness of the material increases and hinders the surface of the material during

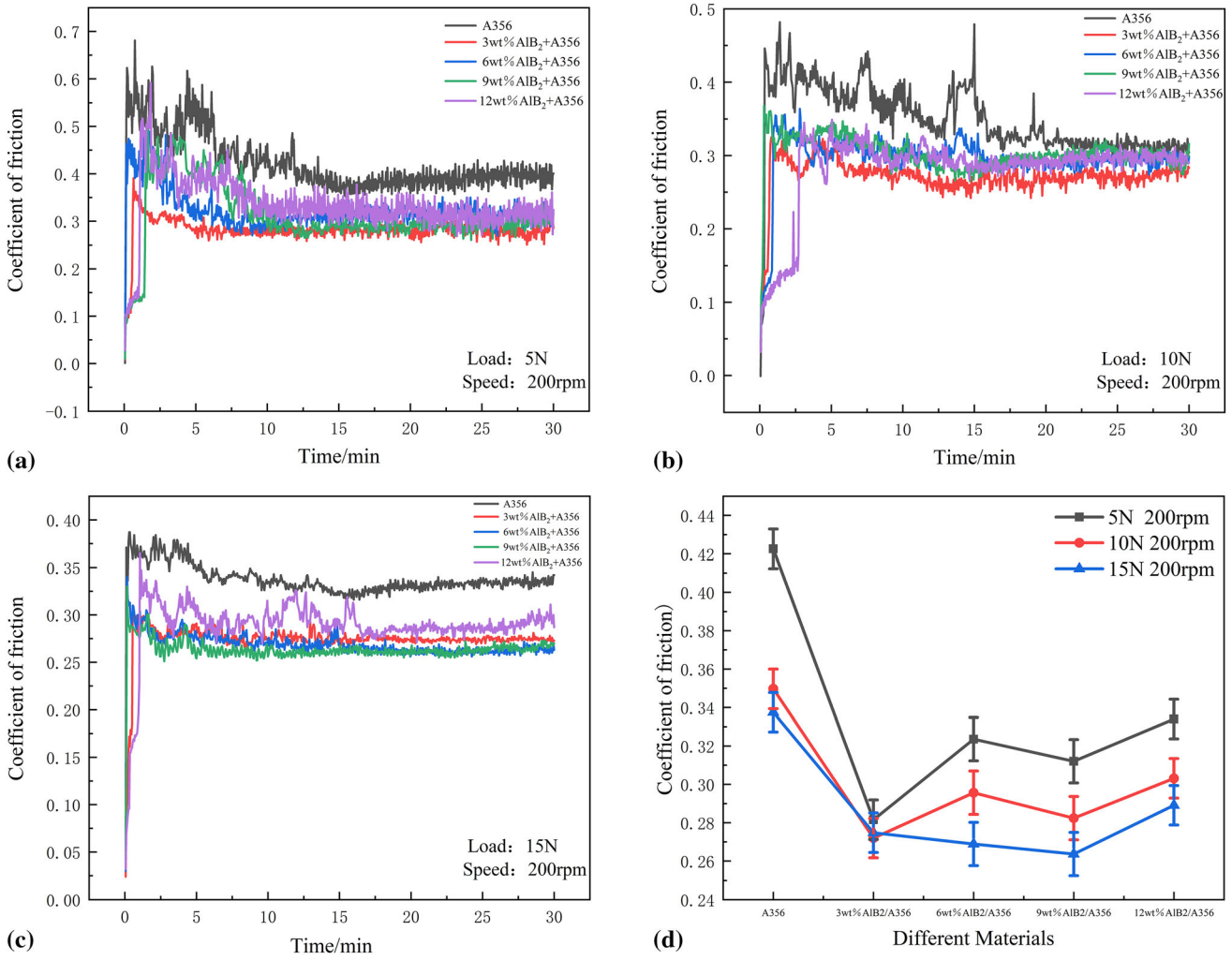

Fig. 6 Coefficient of friction of the matrix and the *x*wt.%AlB2/A356 composite under different load (a) 5N 200rpm; (b) 10N 200rpm; (c)15N 200rpm; (d) Average friction coefficient

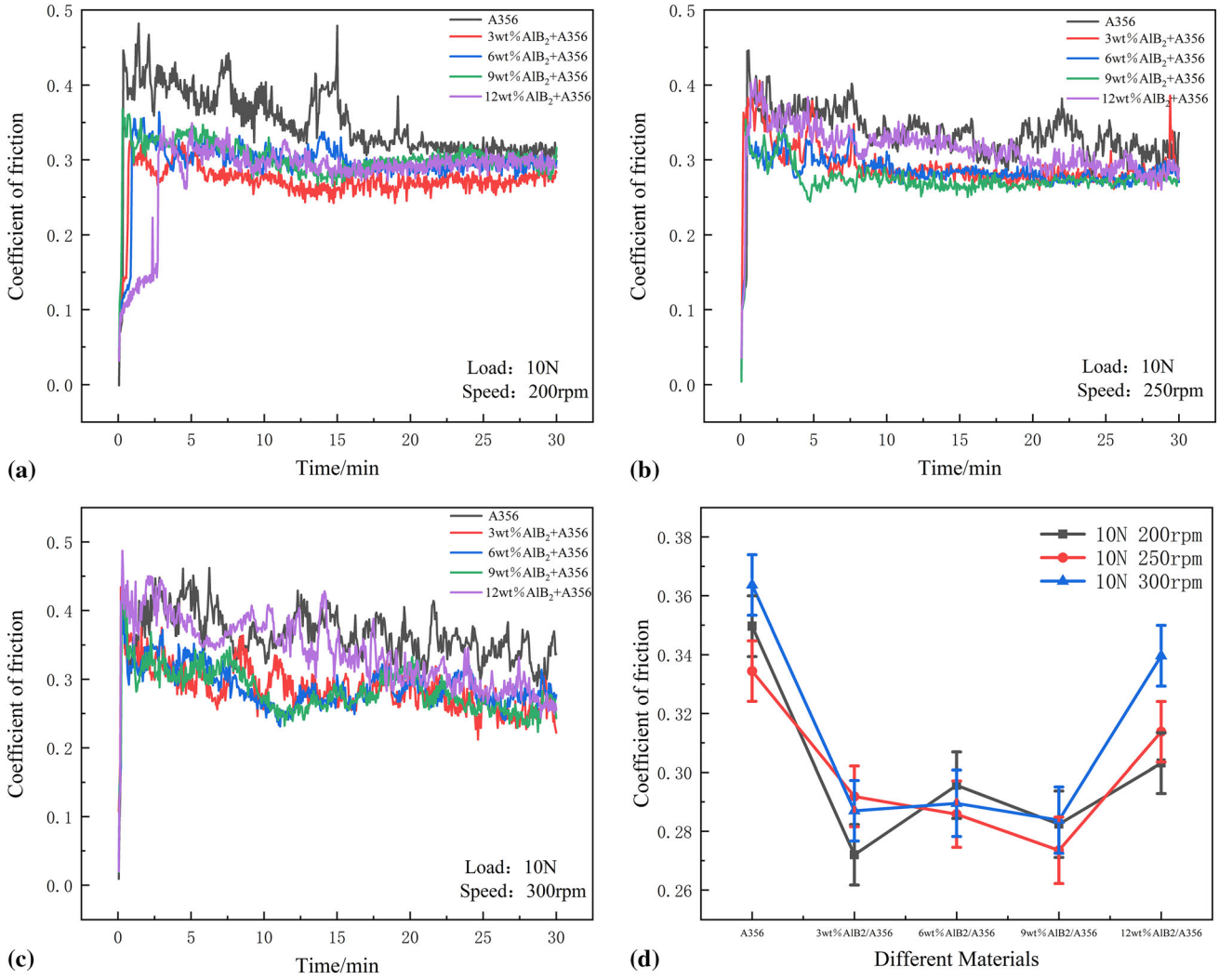

Fig. 7 Coefficient of friction of the matrix and the *x*wt.%AlB2/A356 composite under different Rotating speed (a) 10N 200rpm; (b) 10N 250rpm; (c) 10N 300rpm; (d) Average friction coefficient

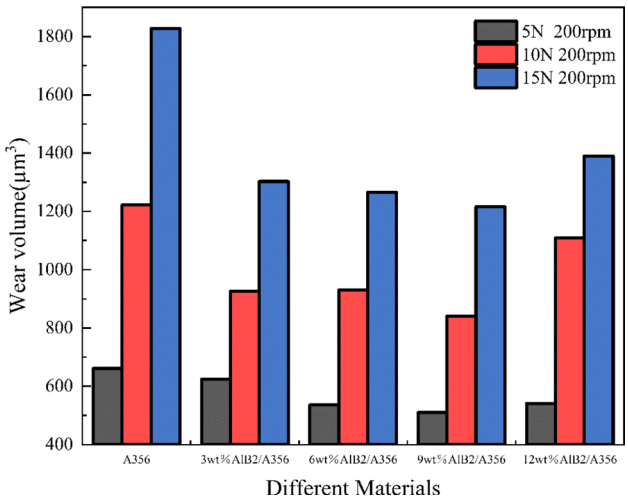

Fig. 8 The wear volume of different materials under different loads

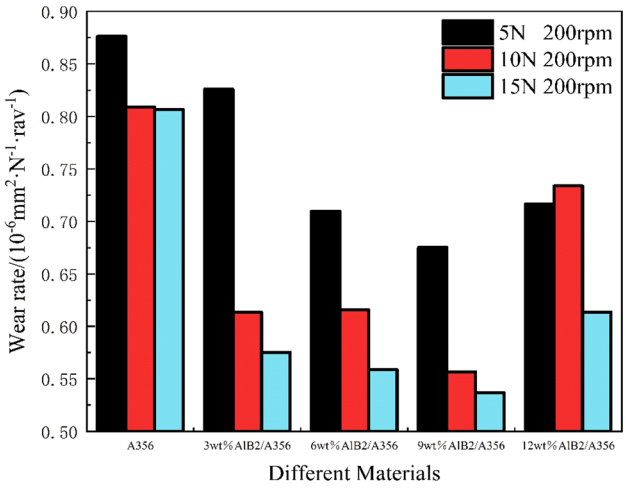

Fig. 9 The wear rate of different materials under different loads

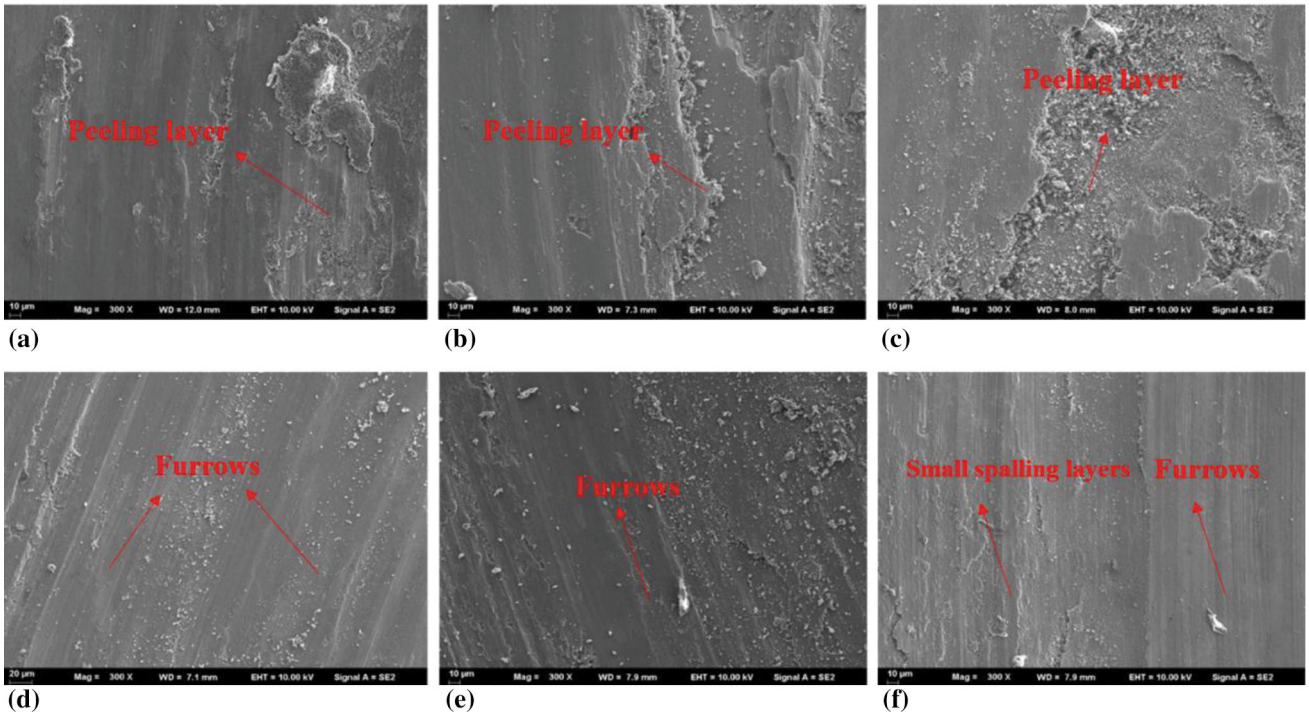

Fig. 10 SEM image of wear morphology of A356 alloy and 9wt.%AlB_2/A356 composite under different loads (a, b, c): A356; (b, c, d): 9wt.%AlB2/A356; (a, e): 5N; (b, f): 10N; (c, g): 15N

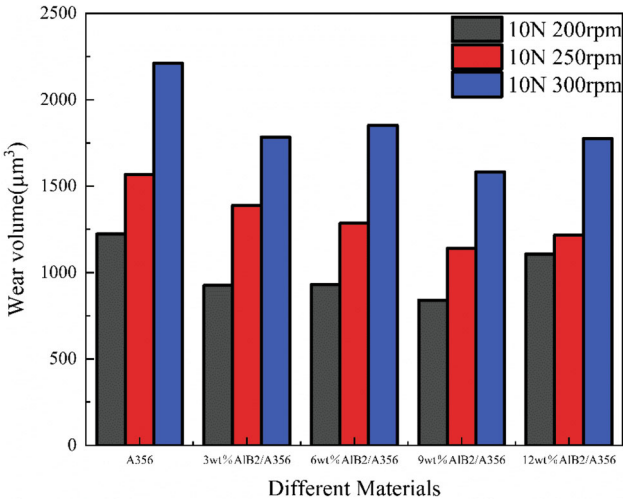

Fig. 11 The wear volume of different materials under different Rotating Speed

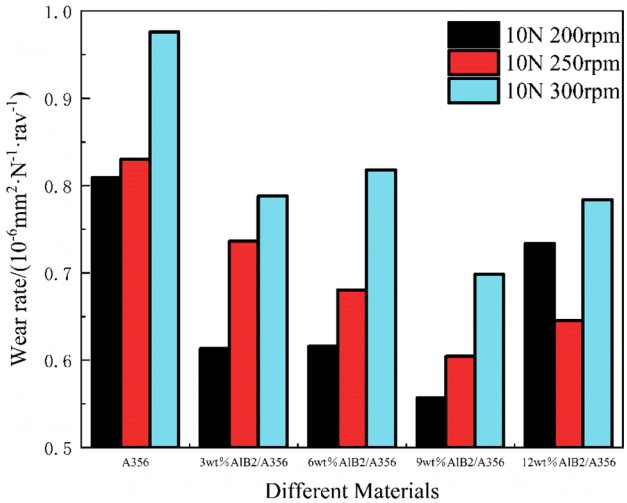

Fig. 12 The wear rate of different materials under different Rotating Speed

wear. Fracture, (2) AlB_2 particles may act as a buffer layer on the surface of the material, which makes the wear strength less than A356 alloy.

3.4 3D Confocal Analysis

Figure 14 and 15 shows 3D confocal observations of the wear surface of the composite material with an AlB2 mass fraction of 9% and the A356 matrix. It can be seen from Fig. 14 that under the condition of 15N, 200rpm, the wear scar depth of the material is reduced from 198.2 μm of the A356 matrix to 100.9 μm of the composite material, a reduction of 49.09%. It can be seen in Fig. 15 that under the condition of 10N, 300 rpm, the wear scar depth of the material is reduced from 267.2 μm of the A356 matrix to 165.8 μm of the composite material, a reduction of 37.94%. It can be seen that the friction and wear behavior of the composite material is greatly improved compared with the A356 matrix under the influence of load or speed.

The friction and wear model of the composite material is shown in Fig. 16. Due to the mechanical alloying mechanism, a mechanical mixing layer (MML) is formed on the worn surface. When a thin layer of MML with higher hardness is formed, the friction performance of the material can be improved. The MML formed by AlB_2 can achieve this effect. It can be seen that when there are AlB_2 particles in the friction material, the

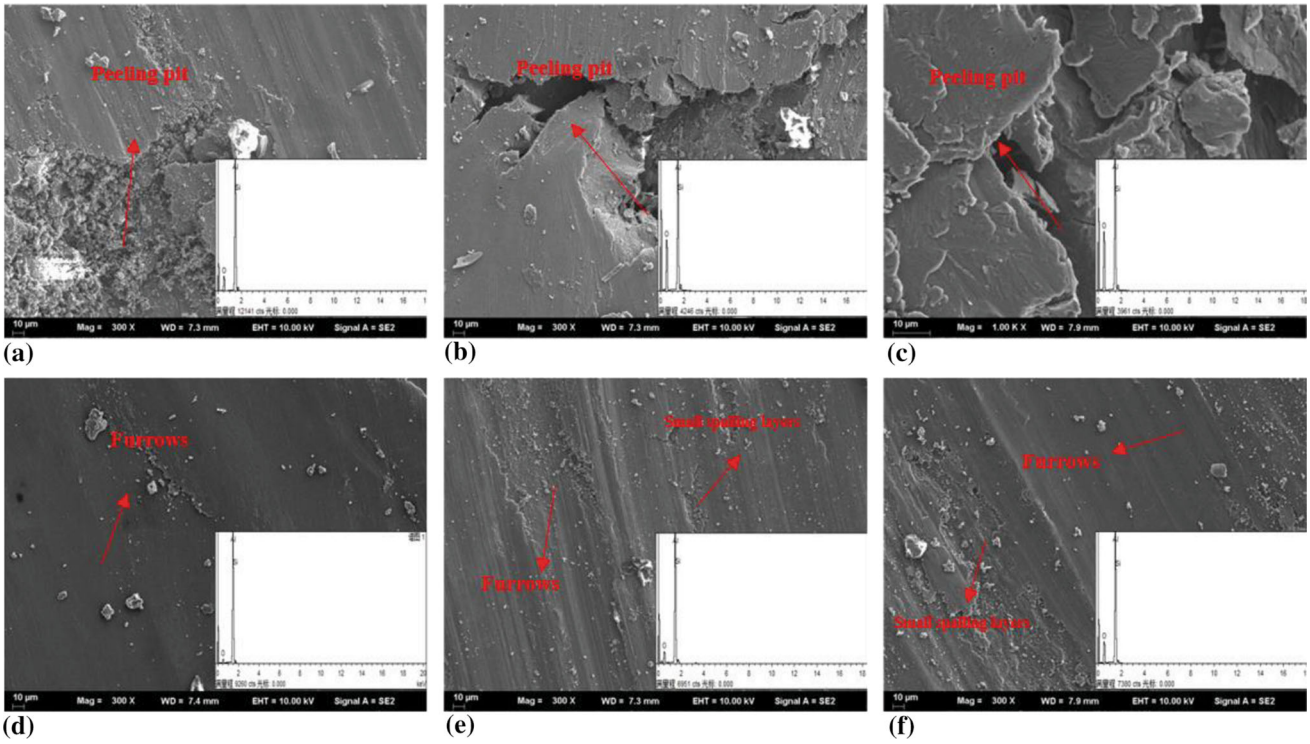

Fig. 13 SEM image of wear morphology of A356 alloy and 9wt.%AlB_2/A356 composite under Rotating Speed (a, b, c: A356; b, c, d: 9wt.%AlB2/A356; a, e: 200rpm; b, f: 250rpm; c, g: 300rpm

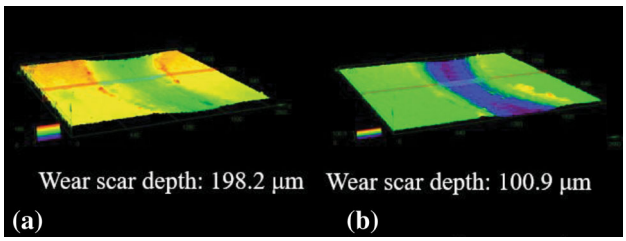

Fig. 14 3D confocal images of wear morphologies of different materials a: A356 b: 9wt.%/A356, 15 N, 200 rpm

MML with micro-protrusions can reduce the friction contact surface, and even play a certain lubricating effect, so that the friction coefficient is reduced and stabilized. This is consistent with the change in the friction coefficient analyzed above, and once again proves that the AlB_2 particles in the composite material can improve the friction performance of the material.

4. Conclusion

Through the in situ reaction of the new A356-KBF_4 system, *x*wt.% AlB_2/A356 (x = 3, 6, 9, 12) particle-reinforced aluminum matrix composites were obtained, and the following conclusions were drawn through data analysis:

(1) XRD analysis and SEM analysis have confirmed that the new A356-KBF4 in situ system can prepare AlB_2 particle-reinforced aluminum matrix composites. MDI Jade 6 software analysis and formula calculation have proved that AlB_2 can be used as an effective nucleation site for aluminum alloy. Observed by polarized light microscope and analyzed by image pro plus software, it is concluded that when x = 9, AlB_2 particles have the most obvious effect on the grain refinement of A356 al-

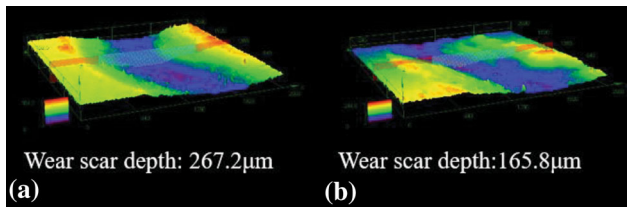

Fig. 15 3D confocal images of wear morphologies of different materials a: A356 b: 9wt.%/A356, 10 N, 300 rpm

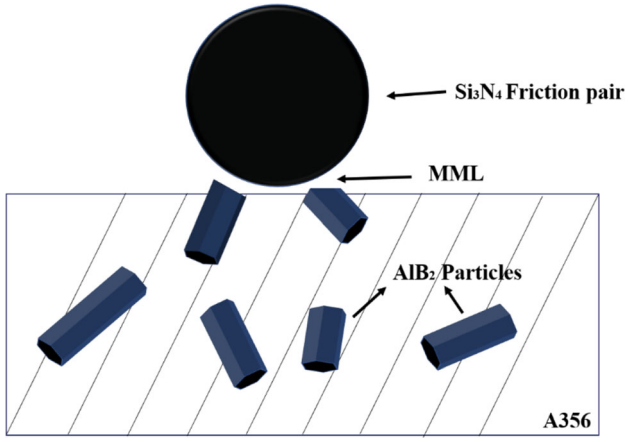

Fig. 16 Tribological behavior model diagram of composites

loy, and the grain size is reduced to an average of 28.5847μm.

(2) Friction and wear tests were carried out on A356 alloy and $x$wt.% AlB_2/A356 composite materials at different speeds and different loads. The test results show that the addition of AlB_2 particles has the effect of reducing friction and enhancing the wear resistance of the material. When $x = 3$, the anti-friction effect is the most obvious reaching 24.7522% (load) and 18.682% (rotation speed), when $x = 9$ the wear resistance of the material reaches the highest level, with an average increase of 29.1974% (load) and 28.9505% relative to the matrix. And the wear mechanism of composite materials is mainly abrasive wear.

(3) Through the 3D confocal observation of the wear surface morphology of the A356 matrix and the composite material, it is found that the wear scar depth of the composite material is much shallower than the wear scar depth of the A356 matrix. Under the condition of 15N, 200rpm, it is reduced by 49.09%. Under the condition of 10N, 300rpm, it is reduced by 37.94%. And by establishing a model to analyze the wear behavior mechanism of composite materials

Acknowledgment

This research was financially supported by the (1) National Natural Science Foundation of China, No. 51605206. (2) National Natural Science Foundation of China, No. U20A20274.(3) National Natural Science Foundation of China, No. 52071158.(4) National Natural Science Foundation of China, No. U1664254.(5) Jiangsu Province key Laboratory of High-end structural Materials, No. hsm180.(6) Innovation Fund of Industrial Center of Jiangsu University,No.ZXJG2020062

References

1. S.R. Sagar, K.M. Srikanth and R. Jayasimha, Effect of Cryogenic Treatment and Heat Treatment on Mechanical and Tribological Properties of A356 Reinforced with SiC, *Mater. Today Proc.*, 2021, **45**, p 184
2. G. Li, W. Jiang, F. Guan, J. Zhu, Y. Yu and Z. Fan, Improving Mechanical Properties of AZ91D Magnesium/A356 Aluminum Bimetal Prepared by Compound Casting Via a High Velocity Oxygen Fuel Sprayed Ni Coating, *J. Magn. Alloys*, 2021 https://doi.org/10.1016/j.jma.2021.02.002
3. J. Xu, G. Chen, Z. Zhang, Y. Zhao, T. Zhang, C. Zhang and D. Ding, Effect of Al-3 wt% Al2O3 Master Alloy Fabricated by Calcined Kaolin on Grain Refinement and Mechanical Properties of A356 Alloy, *J. Alloys Comp.*, 2021, **862**, p 158512.
4. B. Chen, X.Y. Zhou, B. Zhang, K. Kondoh, J.S. Li and M. Qian, Microstructure, Tensile Properties and Deformation Behaviors of Aluminium Metal Matrix Composites Co-Reinforced by Ex-Situ Carbon Nanotubes and In-Situ Alumina Nanoparticles, *Mater. Sci. Eng. A*, 2020, **795**, p 139930.
5. R. Tao, Y. Zhao, X. Kai, Z. Zhao, R. Ding, L. Liang and W. Xu, Microstructures and Properties of In Situ ZrB 2 /AA6111 Composites Synthesized Under a Coupled Magnetic and Ultrasonic Field, *J. Alloy. Compd.*, 2018, **754**, p 114–123.
6. S.L. Lijun Zu*, Study on the Powder Mixing and Semi-Solid Extrusion Forming Process of SiCp/2024Al Composites. J. Mater. Process. Technol. (2001), 114, 189-193
7. J. Chen and X. Gao, Thermal and Electrical Anisotropy of Polymer Matrix Composite Materials Reinforced with Graphene Nanoplatelets and Aluminum-Based Particles, *Diamond Relat. Mater.*, 2019, **100**, p 107571.
8. M.B.A. Shuvho, M.A. Chowdhury, M. Kchaou, B.K. Roy, A. Rahman and M.A. Islam, Surface Characterization and Mechanical Behavior of Aluminum Based Metal Matrix Composite Reinforced with Nano Al2O3, SiC, TiO2 Particles, *Chem. Data Collect.*, 2020, **28**, p 100442.
9. G. Chen, J. Wan, N. He, H.-M. Zhang, F. Han and Y.-M. Zhang, Strengthening Mechanisms Based on Reinforcement Distribution Uniformity for Particle Reinforced Aluminum Matrix Composites, *Trans. Nonferrous Metals Soc. China*, 2018, **28**(12), p 2395–2400.
10. L. Ma, C. Zhou, Q. Wen, M. Li, H. Zhong and S. Ji, Ultrasonic-Promoted Rapid Transient Liquid Phase Bonding of High Volume Fraction SiC Particle Reinforced Aluminum-Based Metal Matrix Composite in Low Temperature, *Ultrasonics*, 2020, **106**, p 106159.
11. S. Ozden, R. Ekici and F. Nair, Investigation of Impact Behaviour of Aluminium Based SiC Particle Reinforced Metal–Matrix Composites, *Compos. A Appl. Sci. Manuf.*, 2007, **38**(2), p 484–494.
12. C. Tom Scaria and R. Pugazhenthi, Effect of Process Parameter on Synthesizing of TiC Reinforced Al7075 Aluminium Alloy Nano Composites, *Mater. Today Proc.*, 2020 https://doi.org/10.1016/j.matpr.2020.07.490
13. S. Sardar, I. Roy, S. Chakraborty, A.B. Ghosh and A. Bandyopadhyay, A Selective Approach Towards Synthesis of Poly (3-bromo thiophene)/Graphene Quantum Dot Composites via In-situ and Ex-situ Routes: Application in Light Emission and Photocurrent Generation, *Electrochim. Acta*, 2020, **365**, p 137369.
14. M.H. Daneshifar, A. Papi and M. Alishahi, Fabrication of Al-Si/Mg2Si in-Situ Composite by Friction Stir Processing, *Mater. Lett.*, 2021, **282**, p 128832.
15. X. Zhang, Y. Sun, M. Niu, M. Shao and X. Geng, Microstructure and Mechanical Behavior of In Situ TiC Reinforced Fe3Al(Fe–23Al–3Cr)Matrix Composites by Mechanical Alloying and Vacuum Hot-Pressing Sintering Technology, *Vacuum*, 2020, **180**, p 109544.
16. R. Wang, W. Guo, J. Wang, K. Yuan, L. Liu, P. Li and Y. Li, Effects of Stress State, Strain Rate, and Temperature on Fracture Behavior of In Situ TiB2/2024 Al Composite, *Mech. Mater.*, 2020, **151**, p 103641.
17. B. Guo, M. Song, X. Zhang, X. Cen, W. Li, B. Chen and Q. Wang, Achieving High Combination of Strength and Ductility of Al Matrix Composite Via In-Situ Formed Ti-Al3Ti Core-Shell Particle, *Mater. Charact.*, 2020, **170**, p 1106666.
18. M. Tayebi, D. Bizari and Z. Hassanzade, Investigation of Mechanical Properties and Biocorrosion Behavior of In Situ and Ex Situ Mg Composite for Orthopedic Implants, *Mater. Sci. Eng. C Mater. Biol. Appl.*, 2020, **113**, p 110974.
19. L. Jiao, L. Fan, Y. Zhao, W. Wang, H. Peng, H. Li, Y. Yong, L. Dong, Microstructure and Tribological Behavior of In Situ ZrB 2 /A356 Composites Prepared Under Magnetic Field. *Surf. Topogr. Metrol. Prop.*, 2021, **9**, p 015026
20. B. Kaveendran, G.S. Wang, L.J. Huang, L. Geng and H.X. Peng, In Situ (Al3Zr+Al2O3np)/2024Al Metal Matrix Composite with Novel Reinforcement Distributions Fabricated by Reaction Hot Pressing, *J. Alloy. Compd.*, 2013, **581**, p 16–22.
21. C. Wu, T. Gao, Q. Sun, G. Liu, X. Du and X. Liu, A novel Method of Coating Ex-Situ SiC Particles with In-Situ SiC Interlayer in Al-Si-C Alloy, *J. Alloy. Compd.*, 2018, **754**, p 39–47.
22. L.-L. Zhang, H.-X. Jiang, J. He and J.-Z. Zhao, Kinetic Behaviour of TiB2 Particles in Al Melt and Their Effect on Grain Refinement of Aluminium Alloys, *Trans. Nonferrous Metals Soc. China*, 2020, **30**(8), p 2035–2044.
23. S. Mozammil, J. Karloopia, R. Verma and P.K. Jha, Effect of Varying TiB2 Reinforcement and its Ageing Behaviour on Tensile and Hardness Properties of In-Situ Al-4.5%Cu-xTiB2 Composite, *J. Alloys Comp.*, 2019, **793**, p 454–466.
24. S. Zhang, Y. Zhao, G. Chen and X. Cheng, (Al2O3+Al3Zr)/A356 Nanocomposites Fabricated by Magnetochemistry in Situ Reaction, *J. Alloy. Compd.*, 2009, **475**(1–2), p 261–267.
25. W. Qian, Y. Zhao, X. Kai, Y. Yan, R. Tao and X. Gao, Synergistic Reinforcement of In Situ (ZrB2+TiB2) Particles and Er on Microstructure and Properties of 6082Al Matrix Composites, *J. Alloys Comp.*, 2020, **813**, p 152198.
26. M.S. Ashok Kumar, C. Honnaiaha and S.L. Ajit Prasad, Influence of Extrusion process on Mechanical and Tribological Properties of Aluminium A356 - AL2O3 Stir Cast MMC, *Mater. Today Proc.*, 2018, **5**(13), p 26918–26924.

27. B. Abbasipour, B. Niroumand, S.M. Monir Vaghefi and M. Abedi, Tribological Behavior of A356−CNT Nanocomposites Fabricated by Various Casting Techniques, *Trans. Nonferrous Metals Soc. China*, 2019, **29**(10), p 1993–2004.
28. M. Janbozorgi, M. Shamanian, M. Sadeghian and P. Sepehrinia, Improving Tribological Behavior of Friction Stir Processed A413/SiC p Surface Composite Using MoS 2 Lubricant Particles, *Trans. Nonferrous Metals Soc. China*, 2017, **27**(2), p 298–304.
29. K.L. Firestein, S. Corthay, A.E. Steinman, A.T. Matveev, A.M. Kovalskii, I.V. Sukhorukova, D. Golberg and D.V. Shtansky, High-Strength Aluminum-Based Composites Reinforced with BN, AlB2 and AlN Particles Fabricated Via Reactive Spark Plasma Sintering of Al-BN Powder Mixtures, *Mater. Sci. Eng. A*, 2017, **681**, p 1–9.
30. S. Koksal, F. Ficici, R. Kayikci and O. Savas, Experimental Optimization of Dry Sliding Wear Behavior of in Situ AlB2/Al Composite Based on Taguchi's Method, *Mater. Des.*, 2012, **42**, p 124–130.
31. A.E. Steinman, S. Corthay, K.L. Firestein, D.G. Kvashnin, A.M. Kovalskii, A.T. Matveev, P.B. Sorokin, D.V. Golberg and D.V. Shtansky, Al-Based Composites Reinforced with AlB2, AlN and BN Phases: Experimental and Theoretical Studies, *Mater. Des.*, 2018, **141**, p 88–98.
32. P. Paulraj and R. Harichandran, The Tribological Behavior of Hybrid Aluminum Alloy Nanocomposites at High Temperature: Role of Nanoparticles, *J. Market. Res.*, 2020, **9**(5), p 11517–11530.